Operando X-ray diffraction and X-ray absorption spectroscopy of zero-strain lithium-ion battery material Li[Li$_{1/3}$Ti$_{5/3}$]O$_4$

For lithium insertion materials for lithium-ion batteries (LIBs), the lattice dimensions are usually altered during the charge and discharge reactions owing to changes in the ionic radius of the redox species, Coulomb repulsion between O^{2-} ions, etc. Among various lithium insertion materials, Li[Li$_{1/3}$Ti$_{5/3}$]O$_4$ (LTO) and related compounds are regarded as zero-strain materials because their cubic lattice parameter (a_c) is maintained at ~8.36 Å throughout the electrochemical reaction [1,2]. This zero-strain character is essential for long-cycle-life LIBs and is currently employed in all-solid-state LIBs, which require a robust interface between the electrodes and electrolyte. However, because of this zero-strain character, the reaction mechanisms of LTO, especially those underlying detailed structural transformations, have not been fully understood for approximately the past thirty years [1].

In contrast to conventional *ex situ* analyses, state-of-the-art *in situ* and *operando* techniques are powerful tools for monitoring electrode materials under operating conditions. Since the early 2010s, we have been developing both a Li cell and an experimental setup to perform a series of *operando* X-ray diffraction (XRD) and X-ray absorption (XAS) spectroscopy at the Toyota beamline, SPring-8 **BL33XU** [3,4]. The *operando* XRD/XAS system consists of a specially designed tapered undulator and servo-motor-driven Si channel-cut monochromator, which enables rapid switching to the desired X-ray energy within ~20 s. We applied the *operando* XRD/XAS technique to LTO together with chemometric analyses and the multivariate curve resolution by alternating least squares (MCR-ALS) method.

Figure 1(a) shows the Rietveld analysis results of the pristine LTO sample. The crystal structure can be assigned to a spinel structure with the $Fd\overline{3}m$ space group, in which Li$^+$ ions occupy tetrahedral 8a and octahedral 16d sites and Ti^{4+} ions occupy the 16d site (see the inset of Fig. 1(a)). Figure 1(b) shows the discharge and charge curves of the LTO/Li cell for the *operando* XRD/XAS measurements. The cell voltage (E) rapidly drops from ~2.8 V to ~1.5 V at the beginning of the discharge reaction and then remains constant (~1.5 V) up to a capacity (Q) of 150 mAh·g^{-1}. The flat E is the signature of a two-phase reaction scheme, although only a linear change in a_c was observed in previous *ex situ* XRD analyses [1]. These electrochemical properties are consistent with those of previous studies [1,2], confirming a homogeneous

electrochemical reaction even in the LTO/Li cell for *operando* XRD/XAS measurements.

Figure 2(a) shows the bond length between Ti and O atoms during the discharge and charge reactions, which were determined by *operando* XRD measurements (d_{Ti-O}^{XRD}). During the discharge reaction, d_{Ti-O}^{XRD} monotonically decreases from ~1.986 Å at 0 mAh·g^{-1} to ~1.984 Å at ~170 mAh·g^{-1} and then rapidly increases to ~1.990 Å at ~220 mAh·g^{-1}. During the charge reaction, d_{Ti-O}^{XRD} almost traces with d_{Ti-O}^{XRD} during the discharge reaction at $Q \geq 170$ mAh·g^{-1}. However, the difference in d_{Ti-O}^{XRD} between the discharge and charge reactions (δd_{Ti-O}^{XRD}) clearly appears below 170 mAh g^{-1}. By contrast, the bond lengths between Ti and O atoms determined by *operando* XAS measurements (d_{Ti-O}^{XAS}) are almost the same between the discharge and charge reactions (Fig. 2(b)), i.e., d_{Ti-O}^{XAS} linearly increases from ~1.95 Å at 0 mAh·g^{-1} to ~2.15 Å at ~170 mAh·g^{-1}, corresponding to the change in the ionic radius of Ti ions. Other differences in the results between XRD and XAS measurements are also observed in the normalized concentration (c) profile obtained by the MCR-ALS analyses. For the *operando* XRD measurements shown in Fig. 2(c), the c profile of LTO-1 (or LTO-2) during the discharge reaction differs from that during the charge reaction, whereas for the *operando* XAS measurements shown in Fig. 2(d), the c profile of LTO-1 (or LTO-2) during the discharge reaction is similar to that during the charge reaction. Here, LTO-1 and LTO-2 represent Li[Li$_{1/3}$Ti$_{5/3}$]O$_4$ and Li$_2$[Li$_{1/3}$Ti$_{5/3}$]O$_4$, respectively. The difference in c between the discharge and charge reactions (δc) is related to δd_{Ti-O}^{XRD}.

To summarize the differences in the results between XRD and XAS measurements, we schematically illustrate the reaction mechanisms occurring in LTO
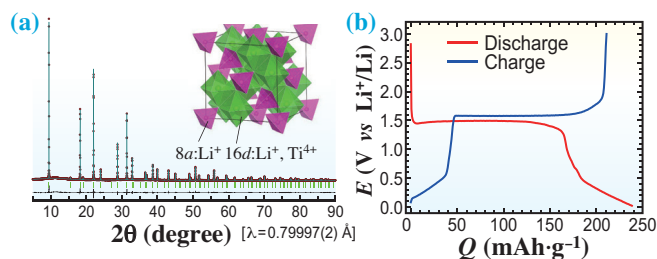

Fig. 1. **(a)** Rietveld analysis results of the pristine LTO sample and a schematic of the crystal structure (inset) and **(b)** discharge and charge curves of the Li/LTO cell for the *operando* XRD/XAS measurements.
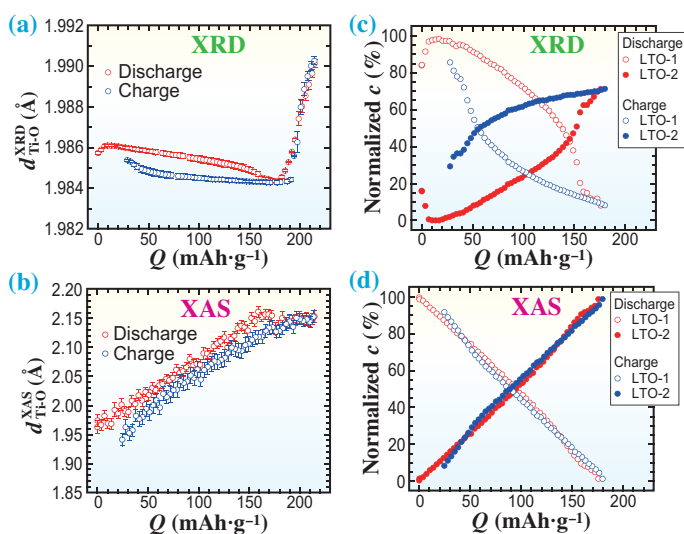
Fig. 2. (a) d_{Ti-O}^{XRD} and (b) d_{Ti-O}^{XAS} during the discharge and charge reactions. Normalized c profiles of the LTO-1 ($Li[Li_{1/3}Ti_{5/3}]O_4$) and LTO-2 ($Li_2[Li_{1/3}Ti_{5/3}]O_4$) components obtained by the MCR-ALS analyses of *operando* (c) XRD and (d) XAS measurements.

at both the micro- (XRD) and atomic (XAS) scales (Figs. 3(a) and 3(b), respectively). The presence of δd_{Ti-O}^{XRD} and δc indicates the difference in the distribution of the LTO-1 (or LTO-2) phase in an LTO particle. During the discharge reaction, Li^+ ions are inserted into the surface, forming a core–shell structure, with the core and shell being LTO-1 and LTO-2, respectively (Fig. 3(a)). During the charge reaction, Li^+ ions are extracted from the surface, forming the opposite core–shell structure. Because the XRD measurements correspond to the core (bulk) structure, δd_{Ti-O}^{XRD} and δc were observed below ~170 mAh·g^{-1}. On the other hand, at the atomic scale

(Fig. 3(b)), Li insertion/extraction proceeds along the two-phase reaction scheme, wherein the amount of LTO-1 (or LTO-2) phase linearly decreases/increases during the discharge and charge reactions.

As described above, we first unveiled the dynamic structural transformations of LTO using this *operando* XRD/XAS technique. The present results would be useful for not only further improving the rate capability of LTO but also clarifying the reaction mechanisms of $LiFePO_4$ and $Li[Ni_{1/2}Mn_{3/2}]O_4$, both of which undergo two-phase reactions. Such studies are underway in our laboratory, and the results will be presented in a forthcoming paper.
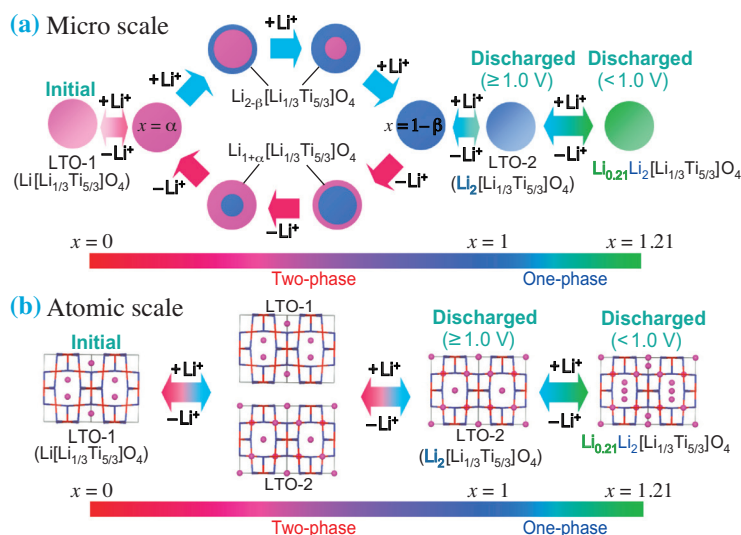

Fig. 3. Schematics of the reaction scheme of LTO at the (a) micro- (<120 nm) and (b) atomic scale (<1 nm) scales. For both scales, the two-and one-phase reaction models are applicable in the x ranges of $0 \leq x \leq 1$ and $1 < x \leq 1.21$, respectively. At the microscale, the $Li_{1+\alpha}[Li_{1/3}Ti_{5/3}]O_4$ (or $Li_{2-\beta}[Li_{1/3}Ti_{5/3}]O_4$) phase is distributed differently in the particle between the discharge and charge reactions, providing δa_c (δd_{Ti-O}^{XRD}) and δc.

Kazuhiko Mukai*, Takeshi Uyama and Takamasa Nonaka

Toyota Central R&D Labs., Inc.

*Email: e1089@mosk.tytlabs.co.jp

References
[1] T. Ohzuku *et al.*: J. Electrochem. Soc. **142** (1995) 1431.
[2] K. Mukai: Inorg. Chem. **58** (2019) 10377.
[3] T. Nonaka *et al.*: Rev. Sci. Instrum. **83** (2012) 083112.
[4] K. Mukai *et al.*: Inorg. Chem. **59** (2020) 16882.
[5] *K. Mukai, T. Nonaka and T. Uyama: Energy Storage Mater.* **44** *(2022) 547.*